CHALMERS
UNIVERSITY OF TECHNOLOGY

A Compact and Wideband MMIC to Ridge Gap Waveguide Contactless Transition for Phased Array Antenna Front-Ends

Citation for the original published paper (version of record):
Vilenskiy, A., Zhang, Y. (2024). A Compact and Wideband MMIC to Ridge Gap Waveguide Contactless Transition for Phased Array
Antenna Front-Ends. IEEE Antennas and Wireless Propagation Letters, 23(3): 990-994.
http://dx.doi.org/10.1109/LAWP.2023.3340876

A Compact and Wideband MMIC to Ridge Gap Waveguide Contactless Transition for Phased Array Antenna Front-Ends

Artem R. Vilenskiy, *Member, IEEE* and Yingqi Zhang, *Student member, IEEE*

***Abstract*—A concept of a contactless in-line transition between a monolithic microwave integrated circuit (MMIC) and a ridge gap waveguide (RGW) is proposed and investigated at W-band. The transition employs an E-plane waveguide bifurcation obtained by mounting a GaAs MMIC on a supporting PCB in the opening of an RGW top metal lid. Designed this way, multiple contactless transitions can be placed in a row with an electrically small spacing that makes the transition idea suitable for array antenna front-ends. A transition equivalent circuit is constructed employing a single-mode transmission line model, which is verified through a full-wave simulation. An (85–105) GHz transition design is then developed and experimentally investigated in the back-to-back configuration indicating a (0.5–0.75) dB transition insertion loss. Finally, the performance of a 1-bit phase shifter MMIC, integrated into the RGW using two proposed transitions, is demonstrated.**

***Index Terms*—Contactless transition, MMIC, gap waveguide, array antennas.**

I. Introduction

RECENTLY, both industrial and academic interest towards high millimeter-wave (mm-wave) frequencies has increased significantly stimulated by emerging communication and sensing radio systems at W- and D-band [1]. In this context, electronically scanned phased array antennas are considered as a key technology enabler providing a high link budget and spatial multiplexing. Numerous efforts have been made to design mm-wave arrays capable of high-efficient and wide-angle beam steering [2]. The most prospective design approaches suggest employing full-metal radiating structures as having the lowest dissipative losses [3], [4], [5]. At the same time, using full-metal waveguide (WG) arrays poses a significant challenge of front-end monolithic microwave integrated circuits (MMICs) integration. The latter is determined by at least two factors: (i) array inter-element spacings are physically small; (ii) any additional interconnecting structures between MMICs and metal WGs are lossy and poorly reproducible.

The problem of MMIC integration has been widely studied in the literature. Formally, the suggested approaches to designing an MMIC-WG transition can be categorized into several groups. The first group encompasses transitions that utilize intermediate printed circuit boards (PCBs), which can be further classified into galvanic contact transitions between a WG and PCB signal lines [6], [7] and contactless designs [8], [9], [10]. Such transitions are prone to PCB substrate losses and require bond wires (BWs) for PCB-MMIC interconnects. In more advanced approaches, the transition is realized directly between a WG and an MMIC through on-chip passive circuitry, thereby minimizing the insertion loss, albeit at the cost of extra MMIC area. In this case, certain designs still incorporate BWs to provide galvanic interconnects [11], [12]. Finally, the most technically advanced solutions utilize contactless direct MMIC-WG transition configurations. One cluster of such designs employs on-chip probes [13] or launchers [14] with orthogonal WGs and in-line transitions, featuring electrically deep coupling cavities [15], [16], which, due to the additional space required for their implementation, are constrained to 1-D arrays. Recently, two compact-sized contactless in-line transitions have been presented. In [17], the authors introduced a resonant transition between a SiGe MMIC and a WG through an H-plane MMIC slot. A useful transition concept was proposed in [18] where they applied an E-plane WG bifurcation for contactless coupling between a ridge WG and an MMIC mounted on the top WG wall.

In this study, we further develop the in-line transition concept based on the E-plane WG bifurcation by presenting a compact and fully functional W-band (85 – 105 GHz) transition design (Fig. 1), where a GaAs MMIC is contactlessly coupled to a ridge gap waveguide (RGW) via an opening in the top RGW metal lid. This RGW structure is employed to construct wideband and wide-angle scanning array antennas at W-band [5]. The arrays feature E- and

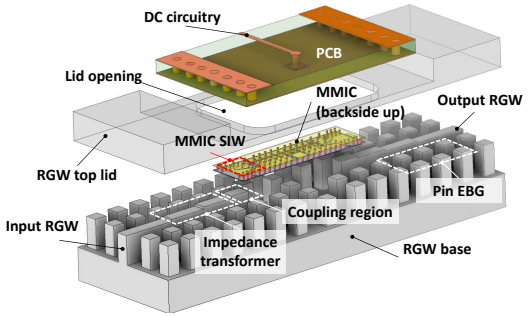

Fig. 1. An exploded view of the proposed MMIC-RGW transition design (B2B configuration).

Manuscript received XX XX, XXXX; accepted XX XX, XXX. Date of publication XX XX, XXX; date of current version XX XX, XXX. This work was carried out in the framework of the EUREKA EURIPIDES2 InnoStar project, Diarienummer 2021-0405, and supported in part by the Swedish Foundation for Strategic Research under Grant STP19-0043. (*Corresponding author: Artem Vilenskiy*, artem.vilenskiy@chalmers.se)

The authors are with Antenna Systems Group, Dept. of Electrical Engineering, Chalmers University of Technology, 41296 Gothenburg, Sweden.

Digital Object Identifier XXXXXX.

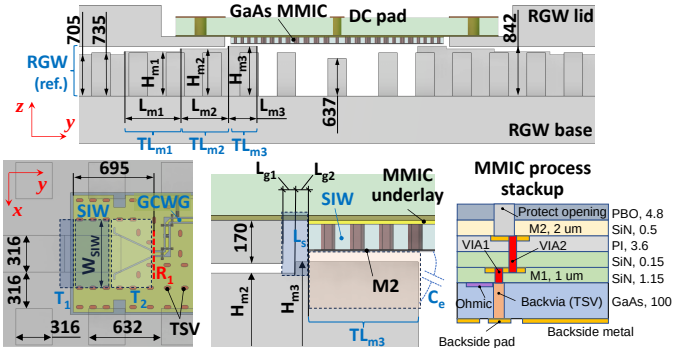

Fig. 2. Detailed views of the transition design: a B2B side view (top), zoomed-in top (bottom left) and side (bottom middle) views of the transition area. The PIH1-10 GaAs MMIC process stackup (bottom right). Unit: μm.

H-plane inter-element spacings of $0.5\lambda_0$ (1.578 mm) and $0.6\lambda_0$ (1.896 mm), λ_0 is the free-space wavelength at the central design frequency $f_0 = 95$ GHz. We introduce an accurate transition equivalent circuit model and validate its performance through a full-wave simulation, discussing crucial aspects of the WG modes transformation between the RGW and an MMIC substrate integrated waveguide (SIW). This model is subsequently employed to optimize the transition design and construct a wideband experimental back-to-back (B2B) prototype. Finally, we demonstrate the design and operation of a completely BW-free 1-bit phase shifter (PS) integrated into the RGW utilizing the proposed transition concept.

II. Transition Design and Equivalent Circuit

A. Design Overview

The exploded view of the B2B structure with two proposed contactless transitions is demonstrated in Fig. 1, while Fig. 2 details its geometric peculiarities. As seen, the transition 2-port network has the input RGW interface. This reference RGW supports the ridge mode with a cut-off frequency of 72 GHz and has the (80 – 160) GHz single-mode operation bandwidth [5], [19], provided by two rows of the pin electromagnetic band gap (EBG) surface. The reference RGW is connected through a 2-step RGW impedance transformer, comprised of two RGW transmission line (TL) segments $TL_{\mathrm{m1,2}}$, to the coupling region interfacing with an MMIC. The GaAs MMIC is mounted (backside up) on a ground plate of the supporting PCB and inserted into the opening of the RGW top metal lid. This way, the PCB ground locally replaces the metal portion of the RGW lid. At the same time, the lossy PCB substrate is fully shielded from the mm-wave field and supports only dc signals. In this study, we use the PIH1-10 PIN-pHEMT GaAs process from WIN Semiconductors, whose stackup is shown in Fig. 2. It offers two gold layers separated by silicon nitride (SiN) and polyimide (PI) dielectrics on a 100 μm GaAs substrate ($\epsilon_r = 12.9$, $\tan(\delta_e) = 0.001$). The process also allows for through-substrate VIAs (TSVs), which we employ to create an SIW by connecting the MMIC backside metal and a top metal plate formed on the metal layer M2 (Fig. 2). By placing the MMIC above the ridge, we split the RGW into the upper SIW and the lower RGW TL_{m3}, formed between the ridge and the M2 metal of the SIW, and thus effectively create

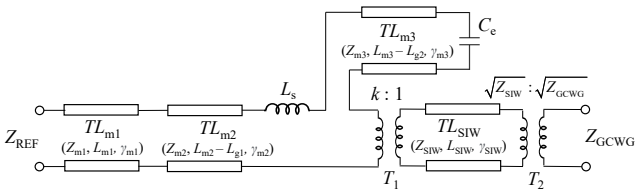

Fig. 3. The equivalent circuit of the transition. Note that the GCWG reference plane is depicted in Fig. 2 as R_1.

an E-plane WG bifurcation [20]. Finally, the on-chip SIW is transformed into the grounded coplanar waveguide (GCWG) through a dual-slot V-shaped transition [21].

When designed this way, multiple MMIC-RGW transitions can be realized by mounting MMICs in a row on a common supporting PCB and directly used in a 1-D (sub-)array front-end [5]. This provides an important advantage over the transition design presented in [18]. The inherently contactless structure of the RGW simplifies MMIC integration.

B. Transition Equivalent Circuit and Design Optimization

Finding a proper transition equivalent circuit provides physical insight into its operation principle and facilitates the impedance matching procedure. Fig. 3 presents the proposed equivalent single-mode 2-port network of the transition. The reference RGW port with the characteristic impedance Z_{REF} is connected to the transformer network composed of TL_{m1} and TL_{m2} having the characteristic impedance $Z_{\mathrm{m1,2}}$ and the complex propagation constant $\gamma_{\mathrm{m1,2}} = \beta_{\mathrm{m1,2}} - j\alpha_{\mathrm{m1,2}}$, where $\beta_{\mathrm{m1,2}}$ and $\alpha_{\mathrm{m1,2}}$ are the phase and attenuation constants. The lid opening forms an equivalent TL impedance step, having the total length of $L_{\mathrm{g1}} + L_{\mathrm{g2}}$, $L_{\mathrm{g1,2}} = 50$ μm, which was chosen to provide a reliable assembling process. This high-impedance region is modeled as the series inductance L_{s}. The bifurcation region is represented by the series connection of TL_{m3}, loaded with the edge capacitance C_{e}, and the SIW, connected through the transformer T_1. The SIW has a set of TL parameters similar to the RGWs. Additionally, the V-shaped SIW-GCWG transition, which exhibits an input reflection coefficient of less than –25 dB, is represented by the transformer T_2 with an ideal voltage transformation ratio of $\sqrt{Z_{\mathrm{SIW}}} : \sqrt{Z_{\mathrm{GCWG}}}$ (where $Z_{\mathrm{GCWG}} = 50$ Ω is the GCWG characteristic impedance).

All TL parameters have been extracted from the full-wave eigenmode analysis in Ansys HFSS. The RGW parts were made of aluminum with the 0.5 μm Groisse surface roughness model. The attenuation constant was defined following [22], [23]: $\alpha = \mathrm{Im}(\hat{f})(\partial \mathrm{Re}(\hat{f})/\partial\beta)^{-1}$, $\hat{f}$ – the eigenmode complex frequency. For the characteristic impedance, the *P-I* definition was employed:

$$Z = \frac{\mathrm{Re}(\iint_S \mathbf{E} \times \mathbf{H}^* d\mathbf{s})}{|\int_l H_x dx|^2}, \tag{1}$$

where $\mathbf{E}$ and $\mathbf{H}$ are the vector modal fields, S is the TL cross-section area, l is the x-oriented line segment crossing the top RGW lid or the SIW metal plate. Taking into account the TE nature of the modes in both TL types, Z can be written in a more explicit form [24]:

$$Z = Z^{\infty} \Big/ \sqrt{1 - (f_c/f)^2}, \tag{2}$$

where Z^{∞} is the high-frequency impedance asymptotics, f_c is the mode cut-off frequency. For the employed SIW TE_{10} mode, these parameters can be found analytically [24], [25]:

$$Z^{\infty}_{\mathrm{SIW}} = \frac{\pi^2}{8}\frac{120\pi}{\sqrt{\epsilon_r}}\frac{H_{\mathrm{SIW}}}{W'_{\mathrm{SIW}}},\ f_c = \frac{c_0}{2W'_{\mathrm{SIW}}\sqrt{\epsilon_r}}. \tag{3}$$

Here, $W'_{\mathrm{SIW}} = W_{\mathrm{SIW}} - D^2/(0.95P)$, $W_{\mathrm{SIW}} = 590\ \ \mu$m and $H_{\mathrm{SIW}} = 105\ \ \mu$m are the SIW width and height (see Fig. 2), $D = 30\ \mu$m, $P = 114\ \mu$m are the SIW TSV width and period, respectively; c_0 is the speed of light in vacuum. The edge capacitance C_{e} is defined through a full-wave simulation for a 1-port open-ended RGW. Finally, having the TL model of the RGW, we can compute the value of L_{s} considering it as an electrically short impedance step [24]:

$$L_{\mathrm{s}} \approx (Z_{\mathrm{g}1}\beta_{\mathrm{g}1}L_{\mathrm{g}1} + Z_{\mathrm{g}2}\beta_{\mathrm{g}2}L_{\mathrm{g}2})/\omega, \tag{4}$$

where $(Z_{\mathrm{g}1,2}, \beta_{\mathrm{g}1,2})$ are the parameters of two RGW segments with $L_{\mathrm{g}1,2}$ (see Fig. 2); ω is the angular frequency. Below, for both C_{e} and L_{s} we use constant values defined at f_0.

The only counterintuitive element of the equivalent circuit is the transformer T_1. Transition full-wave simulations indicated that the RGW experiences a loading from the SIW side lower than Z_{SIW}. This can be explained as an effect associated with the RGW-SIW mode transformation. The SIW cross-section only partially overlaps with the narrower ridge, and only a portion of the SIW magnetic field effectively interacts with the RGW field. Therefore, the transition region equivalently operates as a step-down impedance transformer. Its transformation ratio k can be defined rigorously through the mode-matching analysis [20]. However, given that the RGW gap field is very close to uniform, the following approximate expression, based on the SIW TE_{10} current ratio, can be used

$$k \approx \frac{\int_{-W_{\mathrm{r}}/2}^{W_{\mathrm{r}}/2}\cos(\pi x/W'_{\mathrm{SIW}})dx}{\int_{-W'_{\mathrm{SIW}}/2}^{W'_{\mathrm{SIW}}/2}\cos(\pi x/W'_{\mathrm{SIW}})dx} = \sin\left(\frac{\pi W_{\mathrm{r}}}{2W'_{\mathrm{SIW}}}\right), \tag{5}$$

where $W_{\mathrm{r}} = 316\ \mu$m is the ridge width. The validity of (5) has been numerically verified for various values of W_{SIW}.

The proposed equivalent circuit was used to optimize transition impedance matching in the (85 – 105) GHz bandwidth. The final simulated performance and optimal transition parameters are demonstrated in Fig. 4. A very good agreement with the full-wave simulation is observed in the targeted bandwidth. The simulated (full-wave) S_{11} magnitude is below –20 dB level, while the insertion loss is below 0.5 dB. The resonance around 80 GHz is associated with reaching the band gap edge of the EBG surface. At lower frequencies, impedance matching is limited by operation in the highly dispersive region near the cut-off of the RGW and SIW. The detuning contribution of L_{s} becomes dominating at higher frequencies. On the other hand, L_{s} helps to significantly reduce the length $L_{\mathrm{m}3}$ (*cf.* [18]). Fig. 5 depicts Z dispersion curves for all TLs. The fact that $Z_{\mathrm{SIW}} > Z_{\mathrm{m}2}$ supports the assumption made above on the physical nature of the transformer T_1.

C. Performance Sensitivity

Contactless transitions are known to be sensitive to design tolerances [14], [18]. In the considered case, the performance

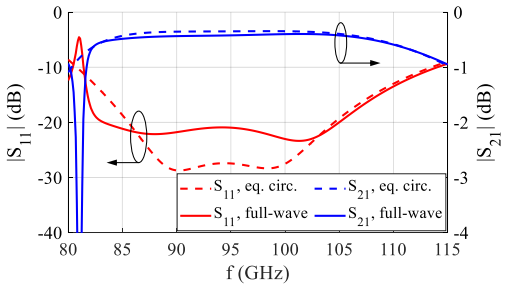

Fig. 4. Transition S-parameters obtained for the equivalent and full-wave models. Final design parameters (μm): $(H_{\mathrm{m}1}, L_{\mathrm{m}1}) = (705, 954)$, $(H_{\mathrm{m}2}, L_{\mathrm{m}2}) = (750, 814)$, $(H_{\mathrm{m}3}, L_{\mathrm{m}3}) = (847, 490)$, $L_{\mathrm{SIW}} = 695$; the MMIC underfill thickness is 20 μm; the transformation ratio $k = 0.78$.

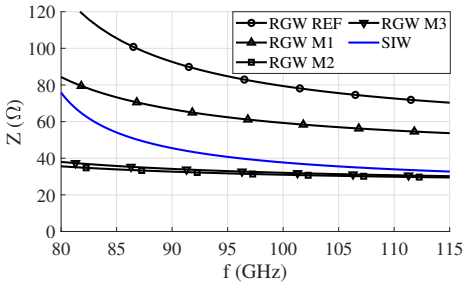

Fig. 5. Dispersion curves of Z computed for the RGWs (Fig. 4) and SIW.

is least affected by an MMIC misplacement in the x-direction: a $\pm 150\ \mu$m shift can be tolerated with $|S_{11}| \leq -15$ dB. An acceptable misplacement along the y-direction is $\pm 50\ \mu$m. The performance is most sensitive to the gap between the ridge and the MMIC (affected by $H_{\mathrm{m}3}$ and the MMIC underfill). In this case, $|S_{11}| \leq -12$ dB is achieved within the range of gap size variation spanning from -30 to 20 μm.

III. Experimental Investigation

A. Back-to-Back Transition Prototype

Several B2B transition prototypes have been manufactured and assembled. Fig. 6(a) shows the mm-wave measurement setup, the assembled B2B structure, and the details of the RGW block. All RGW parts were CNC-milled from aluminum and connected to the measurement equipment through an orthogonal transition between the standard WR-10 WG and the reference RGW. The PCB was made of a 0.2 mm-thick gold-plated FR4 core. Six B2B prototypes were assembled using a standard industrial vacuum pick-and-place process to mount the MMICs with a silver-filled epoxy underfill [Fig. 6(b)]. Each MMIC has two transition structures and a 2.8 mm-long GCWG line.

Measured and simulated S-parameter magnitudes are shown in Fig. 7(a). Note that we subtracted the insertion loss of the feeding RGW TL and orthogonal transitions using an additional through calibration fixture. The measured $|S_{11}|$ is well below the –10 dB level, except for the narrowband region around 89 GHz. The main reasons for this discrepancy are not calibrated out reflections of the orthogonal transitions and assembly errors ($-6\ \mu$m for $H_{\mathrm{m}3}$ and $\pm 8\ \mu$m for the underfill thickness). Overall, the measured $|S_{21}|$ curves are in good agreement with the simulation evidencing the 0.5 – 0.75 dB single transition insertion loss in the targeted bandwidth.

TABLE I. Performance comparison of the reported in-line contactless MMIC-WG transitions.

Ref.	Implementation technology	Bandwidth, GHz	Insertion loss, dB	S_{11}, dB (B2B)	Transv. size, λ_0^2	Bond wires
[16]	Cavity probe, SiGe MMIC + ridge WG (brass), passive	69–90 (26%)	1.5 – 1.7	≤ -10	0.9×0.66	Dc biasing
[17]	H-plane MMIC slot, SiGe MMIC + rect. WG (gold), active	135 – 160 (17%)	4.2 – 5.5	≤ -5	0.81×0.4	Dc biasing
[18]	E-plane bifurcation, Al_2O_3 PCB + ridge WG (aluminum), passive	75 – 110 (38%)	0.7 – 1	≤ -7	$\geq$ 0.93×0.52	Dc biasing
This work	**E-plane bifurc., GaAs MMIC + RGW (aluminum), active**	**85 – 105 (21%)**	**0.5 – 0.75**	≤ -10	**0.6×0.47**	**BW-free**

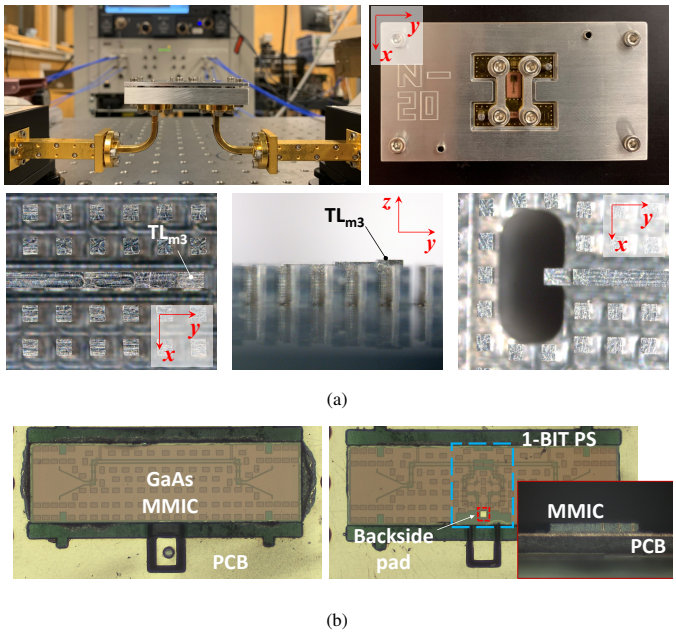

Fig. 6. Photographs of the experimental B2B transition prototype. (a) The measurements setup, the assembled B2B design, and RGW microphotographs. (b) Microphotographs of the B2B transition MMIC (left) and the 1-bit PS with the transitions (right). The inset shows the structure cross-section.

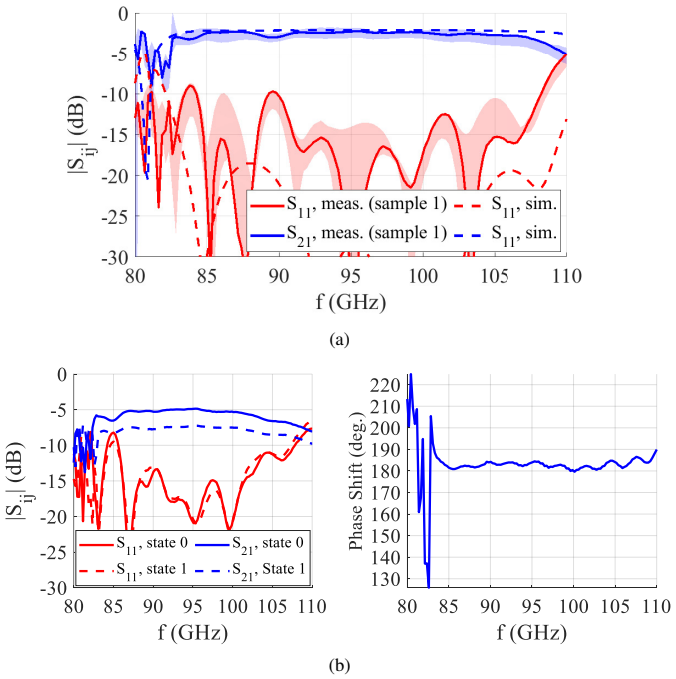

Fig. 7. (a) Comparison between measured and simulated performance of the B2B transition structure (the colored areas depict curve envelopes for 6 measured samples). (b) Measured performance of the 1-bit *p-i-n* diode PS.

B. Integrated 1-Bit Phase Shifter

A 1-bit (180°) *p-i-n* diode PS was designed in the same MMIC process [26] and integrated with two proposed contactless transitions [Fig. 6(b)]. The MMIC dc bias was applied through a backside MMIC pad, *i.e.*, realizing an inverted flip chip MMIC-PCB interconnect. The measured performance [Fig. 7(b)] perfectly agrees with the on-wafer measured results [26] for both S-parameter magnitudes and the expected 180° phase shift.

Table I summarizes the performance of the published in-line contactless transitions potentially suitable for array antenna front-ends. The design reported in [16] features the largest transverse sizes due to the required coupling cavity. The H-plane slot transition from [17] has the resonant performance and is prone to high substrate and surface-wave losses. Finally, the transition concept based on the E-plane WG bifurcation in [18], where an MMIC is mounted directly on the top WG wall, exhibits limitations in terms of impedance matching and is not directly compatible with practical MMICs requiring dc biasing. As seen, the proposed concept demonstrates a state-of-the-art combination of insertion loss and bandwidth. To the best of the authors' knowledge, it is the first presented contactless design suitable for direct integration into 1-D and 2-D array antenna front-ends at W-band, owing to its compact transverse size and completely BW-free implementation.

IV. Conclusion

In this paper, the concept of the contactless in-line MMIC-WG transition based on the E-plane WG bifurcation was further developed to the form suitable for application in high mm-wave array antenna front-ends. We have demonstrated the contactless coupling between the GaAs MMIC and the RGW occupying only the $0.6 \times 0.47\ \lambda_0^2$ transverse WG area. The straightforward and accurate transition equivalent circuit has been introduced, validated through numerical simulations, and used for the development of the (85 – 105) GHz transition design, achieving the (0.5 – 0.75) dB insertion loss. The proposed concept can be readily utilized with front-end array antenna MMICs providing their WG integration in a compact and completely BW-free manner.

Acknowledgment

The authors would like to thank WIN Semiconductors Corporation for fabricating the circuits as a part of WIN's university MPW program. The authors also express gratitude to Thomas Emanuelsson and Richard Lindman (Ericsson AB, Sweden), and Mahdad Sadeghi (MC2, Chalmers University) for their help in MMIC processing and mounting.

REFERENCES

[1] T. S. Rappaport, Y. Xing, O. Kanhere, S. Ju, A. Madanayake, S. Mandal, A. Alkhateeb, and G. C. Trichopoulos, "Wireless communications and applications above 100 GHz: Opportunities and challenges for 6G and beyond," *IEEE Access*, no. 7, pp. 78 729–78 757, 2019.

[2] M. V. Ivashina, A. R. Vilenskiy, H.-T. Chou, J. Oberhammer, and M. Ng Mou Kehn, "Antenna technologies for beyond-5G wireless communication: Challenges and opportunities," in *Proc. 2021 International Symposium on Antennas and Propagation (ISAP)*, Taipei, Taiwan, 2021, pp. 1–2.

[3] A. Gomez-Torrent, M. Garcia-Vigueras, L. Le Coq, A. Mahmoud, M. Ettorre, R. Sauleau, and J. Oberhammer, "A low-profile and high-gain frequency beam steering subterahertz antenna enabled by silicon micromachining," *IEEE Trans. Antennas Propag.*, vol. 68, no. 2, pp. 672–682, 2020.

[4] J. W. Jordan, S. Lynch, M. Clark, B. L. Cannon, L. A. Adames, D. Wrenn, K. Jackson, N. Erickson, J. Clough, D. Brown, J.-M. Rollin, P. Lopez, P. Boutet, and M. Moretto, "Monolithically fabricated 4096-element,PolyStrata® broadband D-band array demonstrator," in *2019 IEEE MTT-S International Microwave Symposium (IMS)*, 2019, pp. 1060–1063.

[5] Y. Zhang, A. R. Vilenskiy, and M. V. Ivashina, "Wideband open-ended ridge gap waveguide antenna elements for 1-D and 2-D wide-angle scanning phased arrays at 100 GHz," *IEEE Antennas Wireless Propag. Lett.*, vol. 21, no. 5, pp. 883–887, 2022.

[6] J. R. Montejo-Garai, L. Marzall, and Z. Popović, "Octave bandwidth high-performance microstrip-to-double-ridge-waveguide transition," *IEEE Microw. Wireless Compon. Lett.*, vol. 30, no. 7, pp. 637–640, 2020.

[7] C. Hannachi, T. Djerafi, and S. O. Tatu, "Broadband E-band WR12 to microstrip line transition using a ridge structure on high-permittivity thin-film material," *IEEE Microw. Wireless Compon. Lett.*, vol. 28, no. 7, pp. 552–554, 2018.

[8] S. R. Zahran, S. Moscato, A. Fonte, M. Oldoni, A. A. Traversa, D. Tresoldi, P. Ferrari, G. Amendola, and L. Boccia, "Flippable and hermetic E-band RWG to GCPW transition with substrate embedded backshort," *IEEE Trans. Microw. Theory Tech.*, vol. 71, no. 6, pp. 2582–2593, 2023.

[9] B. Yuan, P. Wu, Z. Yu, and C. Hao, "Wideband end-wall transition from microstrip to waveguide with via-less choke structure for terahertz application," *IEEE Trans. Terahertz Sci. Technol.*, vol. 12, no. 3, pp. 317–320, 2022.

[10] C. Wang, Y. Yao, J. Wang, X. Cheng, J. Yu, and X. Chen, "A wideband contactless CPW to W-band waveguide transition," *IEEE Microw. Wireless Compon. Lett.*, vol. 29, no. 11, pp. 706–709, 2019.

[11] P. Stärke, C. Carta, and F. Ellinger, "Direct chip-to-waveguide transition realized with wire bonding for 140–220 GHz G-band," *IEEE Trans. Terahertz Sci. Technol.*, vol. 10, no. 3, pp. 302–308, 2020.

[12] J.-L. A. Lijarcio, A. Vosoogh, V. Vassilev, J. Yang, T. Emanuelsson, I. Andersson, and A. U. Zaman, "Substrate-less vertical chip-to-waveguide transition for W-band array antenna integration," in *2023 17th European Conference on Antennas and Propagation (EuCAP)*, 2023, pp. 1–3.

[13] A. Hassona, V. Vassilev, A. U. Zaman, Y. Yan, S. An, Z. S. He, O. Habibpour, S. Carpenter, M. Bao, and H. Zirath, "Nongalvanic generic packaging solution demonstrated in a fully integrated D-band receiver," *IEEE Trans. Terahertz Sci. Technol.*, vol. 10, no. 3, pp. 321–330, 2020.

[14] Q. Ren, C. Bencivenni, G. Carluccio, H. T. Shivamurthy, A. De Graauw, F. Jansen, J. Yang, and A. U. Zaman, "Gapwaveguide automotive imaging radar antenna with launcher in package technology," *IEEE Access*, vol. 11, pp. 37 483–37 493, 2023.

[15] U. Nandi, A. U. Zaman, A. Vosoogh, and J. Yang, "Millimeter wave contactless microstrip-gap waveguide transition suitable for integration of RF MMIC with gap waveguide array antenna," in *2017 11th European Conference on Antennas and Propagation (EUCAP)*, 2017, pp. 1682–1684.

[16] A. Aljarosha, P. Kaul, A. B. Smolders, M. K. Matters-Kammerer, and R. Maaskant, "Silicon-based IC-waveguide integration for compact and high-efficiency mm-wave spatial power combiners," *IEEE Trans. Compon. Packag. Manuf. Technol.*, vol. 11, no. 7, pp. 1115–1121, 2021.

[17] J. Campion, A. Hassona, Z. S. He, B. Beuerle, A. Gomez-Torrent, U. Shah, S. Vecchiattini, R. Lindman, T. S. Dahl, Y. Li, H. Zirath, and J. Oberhammer, "Toward industrial exploitation of THz frequencies: Integration of SiGe MMICs in silicon-micromachined waveguide systems," *IEEE Trans. Terahertz Sci. Technol.*, vol. 9, no. 6, pp. 624–636, 2019.

[18] A. Aljarosha, A. U. Zaman, and R. Maaskant, "A wideband contactless and bondwire-free MMIC to waveguide transition," *IEEE Microw. Wireless Compon. Lett.*, vol. 27, no. 5, pp. 437–439, 2017.

[19] A. R. Vilenskiy, Y. Zhang, and M. V. Ivashina, "Methods for attenuating and terminating waves in ridge gap waveguide at W-band: Carbon-loaded foam, carbonyl iron paint, and nickel plating," in *Proc. 51 European Microwave Conference (EuMC)*, 2021, pp. 1–4.

[20] R. Mittra and S. W. Lee, *Analytical techniques in the theory of guided waves*. Macmillan, New York, 1971.

[21] F. Taringou, D. Dousset, J. Bornemann, and K. Wu, "Substrate-integrated waveguide transitions to planar transmission-line technologies," in *2012 IEEE/MTT-S International Microwave Symposium Digest*, 2012, pp. 1–3.

[22] H. Hsu, "On the general relation between α and Q (correspondence)," vol. 11, no. 4, pp. 258–258, 1963.

[23] V. I. Litun, J. Tharp, and S. L. Chernyshev, "Eigenmode analysis for periodic transmission lines characterization," in *2021 Antennas Design and Measurement International Conference (ADMInC)*, 2021, pp. 48–50.

[24] D. M. Pozar, *Microwave Engineering*. Hoboken, NJ :Wiley, 2012.

[25] Y. Cassivi, L. Perregrini, P. Arcioni, M. Bressan, K. Wu, and G. Conciauro, "Dispersion characteristics of substrate integrated rectangular waveguide," *IEEE Microw. Wireless Compon. Lett.*, vol. 12, no. 9, pp. 333–335, 2002.

[26] A. R. Vilenskiy, Y. Zhang, V. Vassilev, V. Chernikov, and M. V. Ivashina, "Wideband reflection-type *p-i-n* diode phase shifters in GaAs MMIC technology at W-band," in *Proc. 18 European Microwave Integrated Circuits Conference (EuMIC)*, 2023, pp. 209–212.